

Global Rotation Equivariant Phase Modeling for Speech Enhancement with Deep Magnitude-Phase Interaction

Chengzhong Wang, Andong Li, *Member, IEEE*, Dingding Yao, and Junfeng Li

Abstract—While deep learning has advanced speech enhancement (SE), effective phase modeling remains challenging, as conventional networks typically operate within a flat Euclidean feature space, which is not easy to model the underlying circular topology of the phase. To address this, we propose a manifold-aware magnitude-phase dual-stream framework that aligns the phase stream with its intrinsic circular geometry by enforcing Global Rotation Equivariance (GRE) characteristic. Specifically, we introduce a Magnitude-Phase Interactive Convolutional Module (MPICM) for modulus-based information exchange and a Hybrid-Attention Dual-FFN (HADF) bottleneck for unified feature fusion, both of which are designed to preserve GRE in the phase stream. Comprehensive evaluations are conducted across phase retrieval, denoising, dereverberation, and bandwidth extension tasks to validate the superiority of the proposed method over multiple advanced baselines. Notably, the proposed architecture reduces Phase Distance by over 20% in the phase retrieval task and improves PESQ by more than 0.1 in zero-shot cross-corpus denoising evaluations. The overall superiority is also established in universal SE tasks involving mixed distortions. Qualitative analysis further reveals that the learned phase features exhibit distinct periodic patterns, which are consistent with the intrinsic circular nature of the phase. The source code is available at <https://github.com/wangchengzhong/RENet>.

Index Terms—Speech enhancement, phase modeling, global rotation equivariance, magnitude-phase interaction, complex-valued neural network.

I. INTRODUCTION

SPEECH enhancement (SE), the process of improving the quality and intelligibility of speech degraded by acoustic distortion, is a critical technology for telecommunications, smart devices, and hearing aids. SE has historically relied on traditional signal processing methods [1], [2]. However, these conventional approaches often struggle in highly non-stationary acoustic environments. The advent of deep learning has precipitated a paradigm shift, redefining SE as a data-driven discipline. State-of-the-art methods typically learn non-linear masking [3] or mapping [4] functions from degraded to clean speech using vast datasets of paired examples. These

This research is partially supported by National Natural Science Foundation of China (No. 12425413, 12574509), Beijing Natural Science Foundation (L257001, L247022), Oriented Project Independently Deployed by Institute of Acoustics, Chinese Academy of Sciences (MBDX202402).

Chengzhong Wang, Dingding Yao and Junfeng Li are with the Key Laboratory of Speech Acoustics and Content Understanding, Institute of Acoustics, Chinese Academy of Sciences, Beijing 100190, China, and also with University of Chinese Academy of Sciences, Beijing 100049, China. (Email: wangchengzhong@hccl.ioa.ac.cn, yaodingding@hccl.ioa.ac.cn, lijunfeng@hccl.ioa.ac.cn)

Andong Li is with the Key Laboratory of Noise and Vibration Research, Institute of Acoustics, Chinese Academy of Sciences, Beijing 100190, China, and also with University of Chinese Academy of Sciences, Beijing 100049, China. (Email: liandong@mail.ioa.ac.cn)

Corresponding Author: Junfeng Li.

data-driven approaches demonstrate superior performance over traditional techniques, particularly in low signal-to-noise ratio conditions and non-stationary degradation [5].

These methods can be broadly categorized into the time and time-frequency domains. Approaches in the T-F domain are often favored for their physical interpretability [6] and robustness in noisy-reverberant scenarios [7]. Historically, T-F domain methods prioritized magnitude processing [5], disregarding phase due to modeling complexities and its assumed insignificance relative to magnitude [8]. However, with a growing understanding of the role phase plays in speech perception, its importance in challenging reverberant and low signal-to-noise ratio (SNR) conditions has become evident [9]. This necessity is further amplified in Universal Speech Enhancement (USE), which encompasses tasks beyond simple additive noise reduction. For instance, in dereverberation, while magnitude-only processing can partially mitigate amplitude-related effects through appropriate compression, it cannot adequately recover the phase information needed to structurally correct these distortions [10]. Similarly, in bandwidth extension, the realistic regeneration of high-frequency components relies heavily on phase continuity to align harmonics and avoid perceptual artifacts [11]. Consequently, phase-aware methods have increasingly been explored [11]–[13], achieving better performance by fully exploiting the phase information inherent in speech signals.

Tracing the evolution of state-of-the-art predictive SE methods reveals a clear progression toward disentangled magnitude and phase modeling. The Complex Two-Stage Network (CTS-Net) [6] pioneered the idea of magnitude estimation and complex refinement, while the Dual-Branch Attention-In-Attention Transformer (DB-AIAT) [14] introduced a parallel decoder paradigm, which was subsequently adopted by works such as CMGAN [15]. Later, parallel Magnitude-Phase estimation Network (MP-SENet) [16] advanced this strategy by explicit phase modeling: it excluded magnitude information from the complex branch to create a dedicated phase decoder regulated by phase-specific loss functions [17]. Despite sharing a similar architectural backbone, MP-SENet achieved significant performance gains from the explicit phase modeling approach. Following MP-SENet and its updated iteration [18], recent works have made significant strides in improving computational efficiency [19], enhancing structural flow between the encoder and decoders [20], and incorporating auxiliary priors [21], [22]. While these contributions have substantially pushed the boundaries of model efficiency and representation capability, the fundamental challenge of intrinsic phase modeling remains relatively less explored.

Specifically, although current decoupled architectures split

magnitude and phase processing, either via a shared bottleneck [18] or parallel streams [11], [13], they limit the handling of phase's distinct structural nature to the loss term [17], treating it merely as a generic data distribution within the network itself. Mathematically, phase resides on a circular manifold, characterized by periodic continuity. In contrast, the fundamental building blocks of commonly used deep networks operate under Euclidean assumptions. Although complex-valued networks [23] avoid the numerical singularity of phase wrapping by predicting Cartesian components, they introduce a subtler geometric mismatch. Standard operations (e.g., biased convolutions) learn a “preferred” orientation in the complex plane even when there is no input. However, the intrinsic geometry of the phase should be insensitive to the global starting position. This topological perspective aligns with the signal processing properties of the analytic speech signal, where applying a global phase rotation alters the waveform shape but preserves the temporal envelope and instantaneous frequency, with indistinguishable perceptual difference [24], [25]. Consequently, extensive literature models phase primarily through its relative structure [26], [27]. By enforcing equivariance, we ensure that the network separates relative phase structure from the absolute phase orientation.

While Zhang et al. [25] previously identified the issue of global phase bias and addressed it via data augmentation to encourage robustness, our approach offers a fundamental improvement. Instead of using data augmentation to make the network insensitive to the coordinate system, we re-design the network inner structure to respect this topological symmetry, treating the phase space as a rotationally symmetric surface via global rotation equivariant (GRE) network design. As a result, the model becomes intrinsically insensitive to absolute phase orientation, eliminating the need to learn this invariance from data. This design effectively creates a “manifold-aware” processing stream that treats absolute phase orientation as arbitrary while rigorously preserving relative structures.

Given that the rotational symmetry of phase is fundamentally distinct from the geometry of magnitude, we propose a Deep Magnitude-Phase Interaction scheme which maintains a dual-stream flow to respect these topological differences while facilitating necessary information exchange between them. We introduce two novel components: the Magnitude-Phase Interactive Convolutional Module (MPICM) and the Hybrid-Attention Dual-FFN (HADF) structure. These modules allow for the rigorous exchange of information without breaking the rotation-equivariant symmetry of the phase stream. Motivated by recent trends in universal speech restoration [28], we evaluate our proposed model across a comprehensive suite of tasks that involve phase recovery with complete or distorted magnitude: phase retrieval, denoising, dereverberation, BWE, and mixed distortions. The main contributions of this paper are summarized as follows:

- We propose a phase manifold-aware framework that strictly enforces Global Rotation Equivariance as a structural inductive bias. This design aligns the network with the intrinsic circular geometry of the phase, effectively resolving the topological mismatch inherent in conventional Euclidean deep networks.

- We devise a Deep Magnitude-Phase Interaction scheme comprising the Magnitude-Phase Interactive Convolutional Module (MPICM) and the Hybrid-Attention Dual-FFN (HADF). These modules enable rigorous interactive information exchange via cross-branch modulus gating and unified attention score domain interaction respectively, while strictly preserving the geometric constraints of the phase stream.
- We demonstrate that our method achieves superior phase modeling accuracy and generalization capability with fewer parameters and comparable computational cost. Notably, it yields up to a 20% decrease of Phase Distance (PD) in phase retrieval and over 0.1 PESQ improvement in zero-shot cross-corpus denoising evaluations. When applied to phase-involved universal speech enhancement task, including denoising, dereverberation, bandwidth extension, and mixed distortions, the proposed equivariant phase modeling demonstrates clear overall advantages, outperforming state-of-the-art baselines and achieving higher phase estimation accuracy.

II. GLOBAL ROTATION EQUIVARIANCE

In this section, we establish the theoretical foundation of our method, defining the mathematical conditions for Global Rotation Equivariance and delimiting its scope relative to time-shift invariance.

A. Definition and Topological Basis

Global rotation Equivariance refers to the symmetry of a function with respect to global phase shifts [29]. Let $\mathbf{x} \in \mathbb{C}^{C \times H \times W}$ denote a complex-valued input tensor with C channels and (H, W) spatial dimensions, and let T_θ be a global rotation operator such that $T_\theta(\mathbf{x}) = \mathbf{x} \cdot e^{j\theta}$ for any angle $\theta \in [0, 2\pi]$. A neural transformation $\mathcal{F} : \mathbb{C}^{(C, H, W)} \rightarrow \mathbb{C}^{(C', H', W')}$ is defined as global rotation-equivariant if and only if it commutes with T_θ :

$$\mathcal{F}(T_\theta(\mathbf{x})) = T_\theta(\mathcal{F}(\mathbf{x})) \iff \mathcal{F}(\mathbf{x} \cdot e^{j\theta}) = \mathcal{F}(\mathbf{x}) \cdot e^{j\theta}. \quad (1)$$

The rationale for imposing this constraint for phase modeling lies in the topological nature of the phase. Unlike magnitude, which resides in Euclidean space, phase is inherently circular, residing on the manifold S^1 . On this manifold, standard Euclidean metrics are ill-defined due to the rotational symmetry. By enforcing $U(1)$ -equivariance, the model aligns with this circular geometry, treating the absolute phase orientation as arbitrary while rigorously preserving the *relative* phase differences such as GD and IP that encode signal structure.

It is important to clarify the physical interpretation of this rotation in the context of analytic speech signal. Preserving the real-valued nature of speech signal requires Hermitian symmetry in the frequency domain ($X[-k] = X[k]^*$). A true global rotation $e^{j\theta}$ across strictly all frequencies would yield a complex time-domain signal. However, modern speech enhancement networks operate on the *single-sided* spectrum, which effectively models the analytic signal. In this domain, applying a global rotation $e^{j\theta}$ corresponds to a constant phase shift of the analytic representation (a fractional Hilbert

transform). Since this operation preserves the signal's temporal envelope and relative phase structure, the absolute phase orientation carries indistinguishable information. Consequently, enforcing global rotation equivariance is physically justified: it prevents the network from wasting capacity on the arbitrary alignment of the carrier, ensuring the learned representations are invariant to the coordinate system of the complex plane.

B. The Scope of Equivariance: Global vs. Frequency-Dependent

It is also critical to distinguish between *Global Rotation* (a constant phase shift $e^{j\theta}$ across frequencies) and *Frequency-Dependent Rotation* (the linear phase ramp $e^{-j\omega\tau}$ induced by a time shift τ). While it is intuitively appealing to assume that speech phase modeling prioritizes time-shift equivariance, we do not use this bias because of modeling capacity: Key structural characteristics of speech, such as onsets, manifest distinct patterns in the frequency-derivative of the phase (Group Delay, GD) [30]. However, these intrinsic group delay patterns are deeply coupled with the linear phase ramps induced by time shifts [31]. Therefore, enforcing equivariance to frequency-dependent rotations would deprive the model of the ability to modify the GD, restricting its expressive power. Therefore, we adopt Global Rotation Equivariance as the maximal valid symmetry that resolves the manifold mismatch without corrupting the capacity of modeling the speech spectrum.

C. Atomic Global Rotation-Equivariant Operations

Constructing a deep GRE architecture requires identifying fundamental mathematical operations that satisfy (1). While not exhaustive, we focus on two classes of atomic operations chosen for their implementation feasibility:

1) *Bias-free Complex-Linear Transformations*: Standard complex-valued linear transformation (including convolution) is inherently rotation-equivariant, provided the additive bias is strictly zero. A non-zero bias term \mathbf{b} breaks symmetry as $\mathbf{W}(\mathbf{x}e^{j\theta}) + \mathbf{b} \neq (\mathbf{W}\mathbf{x} + \mathbf{b})e^{j\theta}$, where \mathbf{x} is the input tensor.

2) *Invariant-Modulated Transformations*: While holomorphic activations are restrictive [32], non-linearities can be introduced by modulating the equivariant feature \mathbf{x} element-wise with a rotation-invariant real-valued tensor $\mathcal{S}(\mathbf{x})$ (where $\mathcal{S}(\mathbf{x}e^{j\theta}) = \mathcal{S}(\mathbf{x})$). The transformation $\mathcal{F}(\mathbf{x}) = \mathbf{x} \odot \mathcal{S}(\mathbf{x})$ preserves overall equivariance:

$$\mathcal{F}(\mathbf{x}e^{j\theta}) = (\mathbf{x}e^{j\theta}) \odot \mathcal{S}(\mathbf{x}e^{j\theta}) = (\mathbf{x} \odot \mathcal{S}(\mathbf{x})) \cdot e^{j\theta}. \quad (2)$$

This principle allows us to incorporate robust non-linear modeling capabilities, ranging from modulus-based gating mechanisms to rotation-invariant attention weights, without corrupting the GRE property.

III. PROPOSED METHOD

A. Network Overview

Fig. 1 illustrates the proposed architecture, which comprises an encoder, a dual-path bottleneck, and a decoder. Unlike prior works that prioritize macro-level topological search [15], [18], [33], our contribution lies in redefining the

fundamental computational basis to enforce global rotation equivariance. Magnitude and phase are treated with distinct streams maintained as real-valued and complex-valued features throughout the network, where phase stream satisfies global rotation equivariance throughout the network. It is achieved via two core innovations: 1) The Magnitude-Phase Interactive Convolutional Module (MPICM), which replaces standard convolution in the encoder and decoder; 2) the Hybrid Attention Dual-FFN (HADF) module which serves as the dual-path bottleneck structure.

1) *Encoder*: The encoder extracts local features using the MPICM as the fundamental operator. Each MPICM takes two streams as input and output. The encoder initiates with a simplified variant of the MPICM, which processes the compressed magnitude spectrum $\mathbf{M} = \mathbf{Y}_m^\alpha \in \mathbb{R}^{1 \times T \times F}$ (with $\alpha = 0.3$) and the complex Cartesian projection of the phase spectrum $\mathbf{P} = \cos \mathbf{Y}_p + i \sin \mathbf{Y}_p \in \mathbb{C}^{1 \times T \times F}$ as the magnitude and phase stream inputs, respectively, where \mathbf{Y} denotes the complex spectrum of degraded speech, T and F denote the time and frequency dimensions of the STFT. This initial layer projects the raw inputs into high-dimensional feature spaces $\mathbb{R}^{C_{\text{mag}} \times T \times F}$ and $\mathbb{C}^{C_{\text{pha}} \times T \times F}$, expanding the channel dimensions to C_{mag} and C_{pha} for the magnitude and phase streams, respectively. Following this expansion, the features enter a Dual-Stream Dilated DenseNet, containing four MPICMs, which processes phase and magnitude features concurrently. Since dense connectivity inherently involves concatenating all preceding feature maps, we explicitly re-organize the order of accumulated channels from the two streams, ensuring that the magnitude and phase channels are strictly aligned for the subsequent MPICMs, as illustrated in Fig. 1 (b). A final MPICM performs down-sampling, reducing the frequency dimension of both streams to $F' = F/2$ to reduce computational cost of the subsequent bottleneck.

2) *Bottleneck*: To capture long-range contextual dependencies, the latent features of each stream are processed by a bottleneck comprising $N = 4$ cascaded Dual-Path blocks. Each dual-path block consists of two serially connected sub-modules: a Time-HADF and a Frequency-HADF. While sharing an identical HADF architecture (detailed in Sec. III-D), these sub-modules operate on orthogonal dimensions to capture axis-specific dependencies alternately. Specifically, denoting the input representation with the shape of $B \times C_{\{\text{mag,pha}\}} \times T \times F'$ where we added the batch dimension B for illustration. This representation is reshaped to $(BF') \times T \times C_{\{\text{mag,pha}\}}$ and processed by the Time-HADF to model temporal dependencies. Subsequently, the features are permuted to $(BT) \times F' \times C_{\{\text{mag,pha}\}}$, allowing the Frequency-HADF to capture global spectral dependencies. This alternating factorization allows the model to learn full-context spectro-temporal interactions efficiently.

3) *Decoder*: The decoder reconstructs the signal from the bottleneck output. It employs a Dual-Stream Dilated DenseNet with the same structure as in the encoder, that operates on the down-sampled resolution, followed by an up-sampling MPICM that restores the original frequency dimension F . The final layers employ real and complex convolutions to get the estimated compressed magnitude and phase spectra from

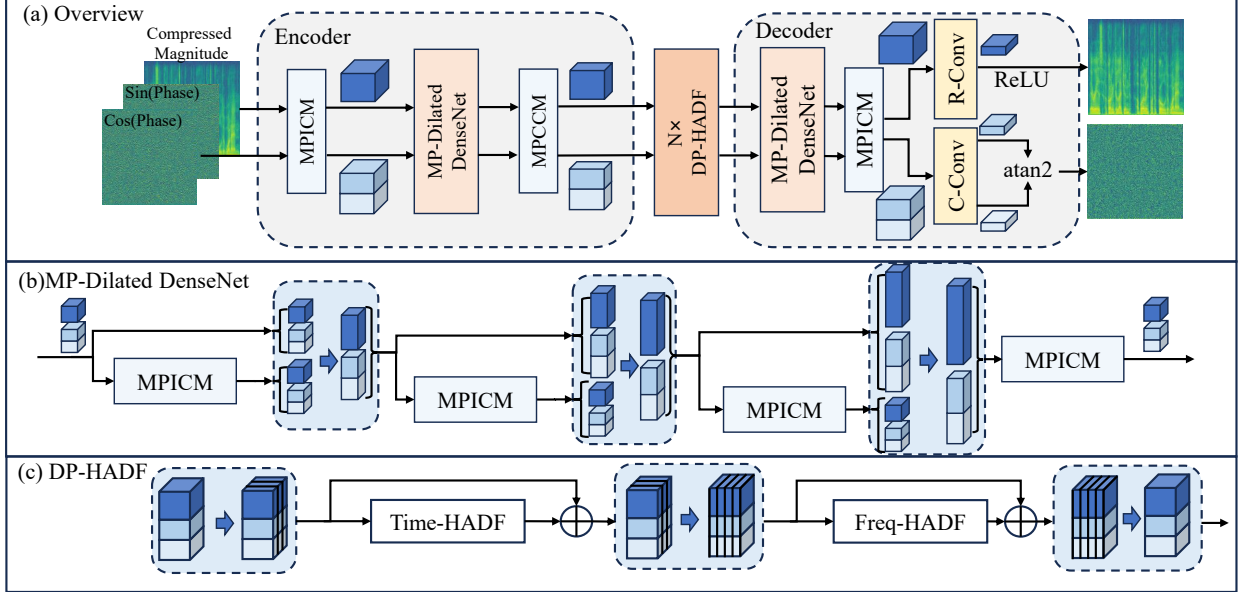


Fig. 1. Overview of the proposed network architecture. (a) The dual-stream encoder-decoder topology. The R-Conv and C-Conv denote real-valued and complex-valued convolution respectively. (b) Structure of the Magnitude-Phase Dilated DenseNet, illustrating the aligned channel concatenation. (c) Signal flow within the dual-path Hybrid-Attention Dual-FFN (HADF) bottleneck.

their respective streams. Specifically, the predicted magnitude is passed through a ReLU activation to enforce non-negativity, while the final phase angle is recovered by applying the arctangent function to the decoded complex phase features.

B. Magnitude-Phase Interactive Convolution Module

The MPICM is designed to process magnitude and phase features in parallel while enforcing geometric constraints. It accepts magnitude M_{in} and phase P_{in} inputs with channel dimension C_{mag}, C_{pha} respectively and spatial dimensions (T, K) , where K adapts to the operating frequency resolution. The workflow is illustrated in Fig. 2, which comprises two stages:

1) *Parallel Feature Extraction*: We extract intra-stream features using distinct architectural paradigms to respect the manifold of each modality.

Phase Stream: To ensure the network learns intrinsic geometric structures, we impose strict rotation equivariance by designing a bias-free and activation-free pipeline. The reason for this design choice is that a fixed bias vector defines a preferred direction in the complex plane, breaking the symmetry required for rotation equivariance, and common complex-valued activations (e.g., ModReLU) often introduce training instability due to undefined gradient regions. We rely on the subsequent gating stage for non-linearity. The intermediate feature is computed as:

$$\tilde{P} = \text{cRMS}_{T'K'}(\text{ComplexConv}(P_{in})). \quad (3)$$

Here, ComplexConv denotes a bias-free complex-valued convolution, mapping the input to the shape of $\mathbb{C}^{C_{pha}^{out} \times T' \times K'}$. In our usage of MPICM, temporal resolution is strictly preserved (i.e., $T' = T$), while the output frequency dimension K' varies according to the module's specific function (maintaining

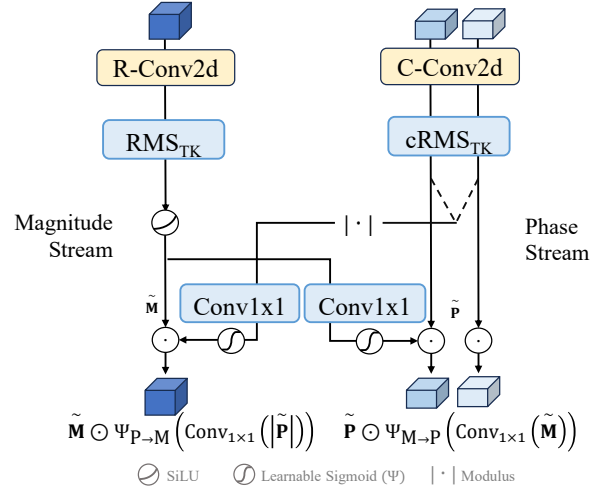


Fig. 2. Detailed structure of the MPICM block, including the magnitude and phase dual-streams and their interaction via the gating mechanism.

$K' = K$ for standard layers, or adjusting appropriately for up-sampling or down-sampling operations). $\text{cRMS}_{T'K'}$ represents Complex RMS Normalization [32] computed over the joint spatial dimensions (T', K') , followed by a frequency-channel-aware learnable scaling vector $\gamma \in \mathbb{R}^{C_{pha}^{out} \times 1 \times K'}$ to capture band-specific importance.

Magnitude Stream: Magnitude spectrum, which directly represents the signal's energy distribution, is naturally suited for conventional neural network pipelines. It applies a 2D convolution followed by RMS Normalization [34] and SiLU activation:

$$\tilde{M} = \text{SiLU}(\text{RMS}_{T'K'}(\text{Conv2d}(M_{in}))), \quad (4)$$

The kernel size, stride, padding and dilation settings of the convolution are identical to that being used in the phase stream, resulting in the feature in $\mathbb{R}^{C_{\text{mag}}^{\text{out}} \times T' \times K'}$. RMS_{TK} : here is the real-valued RMSNorm computed over spatial dimensions, and includes standard learnable affine parameters (scale γ and bias β both in $\mathbb{R}^{C_{\text{mag}}^{\text{out}} \times 1 \times 1}$) applied channel-wise.

2) *Interactive Gating*: To enable cross-modal information flow without violating the rotation equivariance of the phase stream, we propose an interactive gating mechanism that operates element-wise on the extracted features $\tilde{\mathbf{M}}$ and $\tilde{\mathbf{P}}$. The phase-to-magnitude gate is derived from the rotation-invariant modulus $|\tilde{\mathbf{P}}|$, while the magnitude-to-phase gate is derived directly from $\tilde{\mathbf{M}}$. This design makes the global rotation in \mathbf{P}_{in} rotate $\tilde{\mathbf{P}}$ but leave the magnitude gate unchanged, which affects nothing to the whole system but just rotating the output phase feature with the same angle. The interaction is defined as:

$$\begin{aligned} \mathbf{M}_{\text{out}} &= \tilde{\mathbf{M}} \odot \Psi_{\mathbf{P} \rightarrow \mathbf{M}} \left(\text{Conv}_{1 \times 1} \left(|\tilde{\mathbf{P}}| \right) \right), \\ \mathbf{P}_{\text{out}} &= \tilde{\mathbf{P}} \odot \Psi_{\mathbf{M} \rightarrow \mathbf{P}} \left(\text{Conv}_{1 \times 1} \left(\tilde{\mathbf{M}} \right) \right). \end{aligned} \quad (5)$$

where $\text{Conv}_{1 \times 1}$ projects the channel dimensions to match the target stream (e.g., $C_{\text{pha}}^{\text{out}} \rightarrow C_{\text{mag}}^{\text{out}}$). $\Psi(\cdot)$ denotes a frequency-channel adaptive gating function:

$$\Psi(\mathbf{X}) = \alpha \cdot \text{sigmoid}(\mathbf{A} \odot \mathbf{X}), \quad (6)$$

where $\mathbf{A} \in \mathbb{R}^{C_{\{\text{mag,pha}\}}^{\text{out}} \times 1 \times K'}$ is a learnable weight tensor allowing channel-frequency-specific calibration, and $\alpha = 3$ is a fixed scaling factor to extend the dynamic range. It should be noticed that the initial MPICM block which expands the magnitude and phase features omits this gating interaction, as the raw input features do not yet possess the abstract-level information required for cross-stream interaction.

C. Hybrid-Attention Dual-FFN (HADF)

The HADF block modulates feature importance via joint magnitude-phase contexts and subsequently activates them using stream-specific non-linearities.

1) *Signal Flow and Structure*: Let $\mathbf{Z}_{\text{mag}} \in \mathbb{R}^{B' \times L \times C_{\text{mag}}}$ and $\mathbf{Z}_{\text{pha}} \in \mathbb{C}^{B' \times L \times C_{\text{pha}}}$ denote the intermediate bottleneck features, where the effective batch size B' absorbs the orthogonal spatial dimension. The block processes these features through two residual sub-layers: a Hybrid Attention layer and a Dual-FFN layer. Both streams employ Pre-Normalization, utilizing standard RMS Norm for magnitude and Complex RMS Norm (cRMS) for phase. The macroscopic signal flow is defined as:

$$\begin{aligned} \mathbf{H}_{\text{mag}}, \mathbf{H}_{\text{pha}} &= \text{HybridAttention}(\text{RMS}(\mathbf{Z}_{\text{mag}}), \text{cRMS}(\mathbf{Z}_{\text{pha}})), \\ \mathbf{Z}_{\text{mag}}, \mathbf{Z}_{\text{pha}} &\leftarrow \mathbf{Z}_{\text{mag}} + \mathbf{H}_{\text{mag}}, \mathbf{Z}_{\text{pha}} + \mathbf{H}_{\text{pha}} \\ \mathbf{F}_{\text{mag}}, \mathbf{F}_{\text{pha}} &= \text{Mag-FFN}(\text{RMS}(\mathbf{Z}_{\text{mag}})), \text{Pha-FFN}(\text{cRMS}(\mathbf{Z}_{\text{pha}})), \\ \mathbf{Z}_{\text{mag}}, \mathbf{Z}_{\text{pha}} &\leftarrow \text{RMS}(\mathbf{Z}_{\text{mag}} + \mathbf{F}_{\text{mag}}), \text{cRMS}(\mathbf{Z}_{\text{pha}} + \mathbf{F}_{\text{pha}}). \end{aligned} \quad (7)$$

where \mathbf{H} and \mathbf{F} denote the outputs of hybrid attention, and FFN layers respectively, both maintaining the same tensor dimensions as the input \mathbf{Z} in each stream. Following the flow diagram illustrated in Fig. 1c, these outputs are fused with the block's initial input via a global residual connection, preserving the original signal information while integrating the learned transformations.

2) *Hybrid Attention Mechanism*: Effective fusion of magnitude and phase presents a unique challenge: the two streams describe the same signal yet resides on incompatible manifolds. To address this, we propose a Hybrid Attention strategy designed to fuse information in the attention score domain rather than the feature domain.

Feature Projection: To enforce manifold constraints, we generate the Query (\mathbf{Q}), Key (\mathbf{K}), and Value (\mathbf{V}) projections for each stream independently. For a given head h , these are computed via *bias-free* linear transformations to preserve the equivariant properties established in Sec. II:

$$\begin{aligned} \mathbf{Q}_{\text{mag}}^{(h)}, \mathbf{K}_{\text{mag}}^{(h)}, \mathbf{V}_{\text{mag}}^{(h)} &= \text{Linear}_{Q, K, V}^{(h)}(\mathbf{Z}_{\text{mag}}), \\ \mathbf{Q}_{\text{pha}}^{(h)}, \mathbf{K}_{\text{pha}}^{(h)}, \mathbf{V}_{\text{pha}}^{(h)} &= \text{ComplexLinear}_{Q, K, V}^{(h)}(\mathbf{Z}_{\text{pha}}). \end{aligned} \quad (8)$$

where the projected feature sets lie in $\mathbb{R}^{B' \times L \times C_{\text{mag_head}}}$ and $\mathbb{C}^{B' \times L \times C_{\text{pha_head}}}$, respectively, with $C_{\text{mag_head}}$, $C_{\text{pha_head}}$ representing the magnitude and phase channel depth allocated to each attention head, respectively.

Unified Scoring: To derive a shared attention map reflecting the joint confidence of both modalities, we fuse the queries and keys in the Cartesian space. For each head h , the complex phase vectors are decomposed and concatenated with the magnitude vectors:

$$\mathbf{Q}^{(h)} = \text{Concat} \left[\mathbf{Q}_{\text{mag}}^{(h)}, \text{Re}(\mathbf{Q}_{\text{pha}}^{(h)}), \text{Im}(\mathbf{Q}_{\text{pha}}^{(h)}) \right], \quad (9)$$

and similarly for $\mathbf{K}^{(h)}$. The shared attention score $\mathbf{S}^{(h)}$ is computed via the standard scaled dot-product:

$$\mathbf{S}^{(h)} = \text{Softmax} \left(\frac{\mathbf{Q}^{(h)}(\mathbf{K}^{(h)})^{\top}}{\sqrt{d_k}} \right), \quad (10)$$

where $\mathbf{S}^{(h)} \in \mathbb{R}^{B \times L \times L}$, $d_k = C_{\text{mag_head}} + 2C_{\text{pha_head}}$ is the dimension of the concatenated vector per head. Notably, this operation mathematically preserves rotation invariance. The contribution of the phase stream to the dot product corresponds to the real part of the Hermitian inner product [35]:

$$\text{Re}(\mathbf{Q}_{\text{pha}}) \cdot \text{Re}(\mathbf{K}_{\text{pha}})^T + \text{Im}(\mathbf{Q}_{\text{pha}}) \cdot \text{Im}(\mathbf{K}_{\text{pha}})^T = \text{Re}(\mathbf{Q}_{\text{pha}} \mathbf{K}_{\text{pha}}^H). \quad (11)$$

Since $\text{Re}((\mathbf{q}e^{j\theta})(\mathbf{k}e^{j\theta})^H) = \text{Re}(\mathbf{q}\mathbf{k}^H)$, global phase rotations cancel out, ensuring the attention scores remain invariant.

Output Projection: The invariant scores $\mathbf{S}^{(h)}$ modulate the independent Value vectors $\mathbf{V}_{\text{mag}}^{(h)}$ and $\mathbf{V}_{\text{pha}}^{(h)}$ separately. The head outputs are concatenated and projected back to the original stream dimensions via stream-specific output projections Linear_O and ComplexLinear_O (where the latter is bias-free), generating the final residuals:

$$\begin{aligned} \mathbf{H}_{\text{mag}} &= \text{Linear}_O \left(\text{Concat}_h(\mathbf{S}^{(h)} \mathbf{V}_{\text{mag}}^{(h)}) \right), \\ \mathbf{H}_{\text{pha}} &= \text{ComplexLinear}_O \left(\text{Concat}_h(\mathbf{S}^{(h)} \mathbf{V}_{\text{pha}}^{(h)}) \right). \end{aligned} \quad (12)$$

3) *Dual-FFN*: We employ a Convolution-based FFN for the phase stream to prioritize local dependency modeling, and a GRU-based FFN for the magnitude stream to capture global sequential relationships. This design is premised on the insight that phase information governs fine-grained temporal

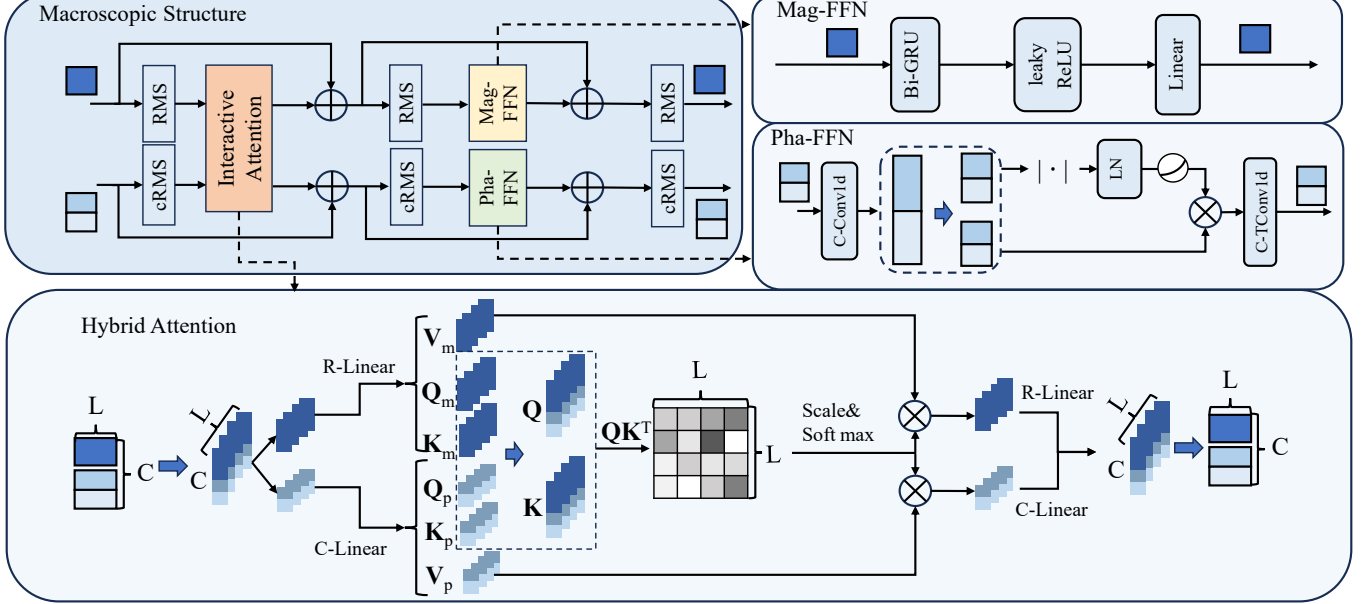


Fig. 3. Detailed architecture of the Hybrid-Attention Dual-FFN (HADF) module. (Top Left) The macroscopic residual block structure. (Bottom) The Hybrid Attention mechanism, illustrating the projection of complex queries/keys into a unified attention map. (Top Right) The distinct feed-forward networks for the magnitude (Mag-FFN) and phase (Pha-FFN) streams.

alignment and local waveform consistency, whereas magnitude information predominates in defining the global spectral envelope and long-range semantic structure.

Magnitude Stream: To capture global sequential dependencies, we adopt a GRU-based architecture as in [18], [36]. This submodule consists of a bidirectional GRU layer that expands the original feature dimension C_{mag} to the hidden dimension $C_{\text{mag_hidden}}$ to capture full-sequence context, followed by a Leaky ReLU activation for non-linearity, and a final linear projection to restore the original channel dimension C_{mag} .

Phase Stream: To capture local geometric structures while enforcing rotation equivariance, we design a complex Gated Linear Unit network. The features are first expanded via a complex convolution and subsequently split into two equal halves, \mathbf{Z}_1 and \mathbf{Z}_2 . Both tensors reside in the complex space $\mathbb{C}^{B' \times L \times C_{\text{pha_hidden}}}$, where $C_{\text{pha_hidden}}$ denotes the expanded channel width. The gating factor is derived solely from the magnitude of \mathbf{Z}_1 , which is then normalized and activated via SiLU to produce a real-valued mask, and scales the complex features of \mathbf{Z}_2 . Finally, a complex projection layer restores the features to original dimension C_{pha} . We denote the sequential processing of the phase stream input \mathbf{Z} as (13):

$$\begin{aligned} [\mathbf{Z}_1, \mathbf{Z}_2] &= \text{Split}(\text{ComplexConv1D}(\mathbf{Z}_{\text{normed_pha}})), \\ \mathbf{F}_{\text{pha}} &= \text{ComplexDeConv}(\mathbf{Z}_1 \odot \text{SiLU}(\text{LayerNorm}(|\mathbf{Z}_2|))). \end{aligned} \quad (13)$$

where \odot denotes element-wise multiplication. Since the gate \mathbf{Z}_g is derived from rotation-invariant moduli, the rotation of the input \mathbf{Z} ($e^{j\theta}$) propagates linearly through \mathbf{Z}_1 and is preserved at the output, satisfying the equivariance condition.

IV. EXPERIMENTAL SETUP

To comprehensively validate the proposed method, we adopt a hierarchical evaluation strategy. We begin by isolating the

model's intrinsic phase modeling capabilities through a dedicated Phase Retrieval task, where the model is provided with the clean compressed magnitude spectrum while the input phase is strictly initialized to zero. After that, we benchmark denoising performance on the standard publicly available VoiceBank+DEMAND [37] and Deep Noise Suppression (DNS) Challenge 2020 [38] datasets. We also perform zero-shot cross-dataset test to verify the generalization ability. Furthermore, to investigate the relative importance of our equivariant phase modeling across various types of degradations, we construct a custom training set derived from DNS 2021 and evaluate performance on a simulated out-of-domain WSJ0+WHAMR! test set and perform ablation studies on it. This custom dataset covers extensive degradations across three representative distortions: denoising, dereverberation, and bandwidth extension, as well as their combinations.

A. Datasets

1) *VoiceBank+DEMAND*: The VoiceBank+DEMAND (VBD) corpus is a typical benchmark for speech denoising, constructed by mixing clean speech from the Voice Bank corpus [39] with diverse acoustic environments from the DEMAND database [40] and artificial noise sources. All audio recordings were downsampled to 16 kHz in our experiment. The training set comprises 11,572 utterances from 28 speakers. We also perform the phase retrieval task on the clean speech partition (VoiceBank corpus [39]), adhering to the standard speaker-disjoint split.

2) *DNS Challenge 2020*: The DNS Challenge-2020 corpus [38] provides over 500 hours of high-quality clean speech from 2,150 distinct speakers and approximately 180 hours of diverse noise clips. Following the official script, we generated a total of 3,000 hours of noisy-clean training pairs, with SNR

levels of noisy speech randomly sampled from a uniform distribution between -5 dB and 15 dB, without reverberation. For evaluation, we utilize the non-reverberant category for official non-blind test set, which consists of 150 synthetic recordings.

3) *DNS-Challenge 2021 + WSJ0-WHAMR!*: We adopt the DNS Challenge 2021 corpus [41] as the training set for our comprehensive speech restoration experiments, which provides a significantly richer set of room impulse responses. The clean speech is exclusively sourced from the `read_speech` subset of DNS 2021. To strictly evaluate out-of-domain generalization, the test set is derived from the `si_et_05` evaluation subset of WSJ0 [42], comprising 651 recordings from eight distinct speakers. Our simulation protocol covers three representative distortion categories:

Denoising (DN): Training samples are generated by mixing clean speech with noise clips randomly sampled from the noise in DNS-2021 corpus at SNRs uniformly distributed between -5 dB and 15 dB. To ensure out-of-domain evaluation, we employ noise recordings exclusively from the WHAMR! [7] test partition. This subset comprises 3,000 distinct clips captured in diverse urban environments (e.g., cafes, restaurants, and bars). We randomly mix them with clean speech at fixed SNR levels of 0, 5, 10, and 15 dB.

Dereverberation (DR): For the training set, we simulate reverberant conditions by convolving clean speech with Room Impulse Responses (RIRs) randomly sampled from the DNS-2021 dataset. For the test set, reverberation is generated using the official WHAMR! simulation script based on the image-source method [43].

Bandwidth Extension (BWE): To simulate bandwidth limitations, we employ a resampling-based strategy. The input signals are downsampled to a target effective sampling rate and subsequently upsampled back to the original resolution (16 kHz). For standalone BWE tasks, we generate samples with effective cutoff frequencies of 2 kHz and 4 kHz.

Composite Distortions: To simulate complex acoustic environments, we combine the standalone tasks into two composite scenarios: DN+DR, and DN+DR+BWE. The noise and reverberation settings remain consistent with their standalone definitions, while the bandwidth extension component is restricted to a 4 kHz cutoff in mixed scenarios to preserve essential spectral cues [28].

The final dataset is balanced uniformly across these categories. The training partition comprises 300 hours of audio. The test set contains 1,250 utterances (250 per category) generated from WSJ0 clean speech. For all noise-inclusive test conditions, samples are evenly distributed across five SNR levels as previously described (-5 to 15 dB in 5 dB intervals), with 50 files allocated to each level.

B. Model and Training Configurations

For STFT configuration, a window size of 25 ms is adopted, with 25% shift between adjacent frames, resulting in $F = 201$ frequency bins. We design two model variants, which is Small for the PR task and Standard for the others, with specific channel configurations detailed in Table I. Given that complex-

valued phase channels require approximately double the computational resources of real-valued magnitude channels, we maintain the phase channel number at roughly half of the magnitude one. We will further investigate the impact of this allocation strategy via ablation studies in Section IV-D.

TABLE I
CHANNEL CONFIGURATIONS FOR THE PROPOSED MODEL VARIANTS.

| Model | C_{mag} | C_{pha} | $C_{\text{mag_head}}$ | $C_{\text{pha_head}}$ | $C_{\text{mag_hidden}}$ | $C_{\text{pha_hidden}}$ |
|----------|------------------|------------------|------------------------|------------------------|--------------------------|--------------------------|
| Small | 32 | 16 | 8 | 6 | 64 | 64 |
| Standard | 48 | 16 | 12 | 6 | 96 | 64 |

We adopt the typical loss configuration from MP-SENet [16] for the pure DN task, with the same coefficients for fair comparison. This objective \mathcal{L}_{DN} aggregates magnitude, complex, time-domain, STFT consistency, and PESQ metric discriminator losses with a phase term \mathcal{L}_{pha} which considers group delay, instantaneous phase and angular frequency [17].

$$\mathcal{L}_{\text{DN}} = 0.9\mathcal{L}_{\text{mag}} + 0.3\mathcal{L}_{\text{pha}} + 0.2\mathcal{L}_{\text{com}} + 0.05\mathcal{L}_{\text{Metric}} + 0.1\mathcal{L}_{\text{con}} + 0.2\mathcal{L}_{\text{time}} \quad (14)$$

To address the enhancement failure of conventional methods in BWE-involved universal SE tasks [28], we augment the objective with a Multi-Period Discriminator (MPD) [11], [44] for all evaluated models. Accordingly, the loss function for the USE task is defined as:

$$\mathcal{L}_{\text{USE}} = \mathcal{L}_{\text{DN}} + 0.05\mathcal{L}_{\text{MPD}}, \quad (15)$$

For the Phase Retrieval task, we switch to a loss term better suited for synthesizing phase from scratch. Following the loss setting in BAPEN [45], this specific loss \mathcal{L}_{PR} emphasizes geometric consistency via an omni-directional phase distortion term and an MPD adversarial term:

$$\mathcal{L}_{\text{PR}} = 2 \cdot 10^4 \mathcal{L}_{\text{omni}} + 1 \cdot \mathcal{L}_{\text{MPD}} \quad (16)$$

While loss configurations varied by task, all models were trained using a batch size of $B = 4$ and the AdamW optimizer ($\beta_1 = 0.8, \beta_2 = 0.99$, weight decay 0.01). We set the initial learning rate to 5×10^{-4} , employing an exponential decay of 0.99 per epoch for DNS-2020 (1M steps) and VoiceBank+DEMAND (500k steps). For the simulated DNS-Challenge 2021 corpus, we utilized a slower decay of 0.999 over 500k steps to accommodate its complex degradation.

C. Evaluation Metrics

We evaluate performance using a comprehensive suite of metrics. To verify phase reconstruction accuracy, we report the Phase Distance (PD) [46] and Weighted Omni-directional Phase Distortion (WPD) [45]. General restoration quality is assessed via standard intrusive metrics: PESQ [47], STOI [48], COVL [49], and SI-SDR [50]. For further evaluation of perceptual naturalness, we utilize the reference-free estimators DNSMOS [51] and UTMOS [52].

V. RESULTS AND ANALYSIS

A. Phase Retrieval

To isolate and validate the model’s intrinsic phase modeling capabilities, we first evaluate performance on the phase retrieval task. Given that only the phase needs to be recovered, we employ the Small configuration of our proposed model. The magnitude stream is not discarded here, since the whole phase stream relies on the magnitude one to get information with the input phase all zeros. The difference is that we don’t decode the magnitude from the final MPICM in Fig. 1. We benchmark against a diverse set of baselines, including the classical Griffin-Lim algorithm [53] and generative DiffPhase [54]. We also include MP-SENet Up. [18] and SEMamba [55] as strong predictive baselines, adapting them for this task by retaining only the phase decoder. To ensure fair comparison, all predictive models adhere to the consistent STFT and loss configurations described in Section IV-B. An exception is made for DiffPhase due to its generative nature, where its original loss and STFT formulation are maintained [54]. Quantitative results are presented in Table II. As observed, despite utilizing only 0.90M parameters and 22.89 GMACs, our method surpasses all baselines in phase estimation precision (PD and WOPD) by a substantial margin, while achieving a marginal improvement in perceptual quality. This result is expected, given that metrics such as PESQ are relatively insensitive to fine-grained phase alignment. Nevertheless, this task serves as a critical benchmark for isolating intrinsic phase modeling capabilities. We attribute the significant increase in phase accuracy to the rotation-equivariant design, which explicitly constrains the high-dimensional latent space to consider the circular topology of phase. In contrast, conventional predictive approaches expend capacity to implicitly learn this geometric structure, potentially limiting their performance.

TABLE II

COMPARISON OF PHASE RETRIEVAL PERFORMANCE ON THE VOICEBANK CORPUS. * DENOTES BASELINES ADAPTED WITH A SINGLE PHASE DECODER, AND GRE DENOTES GLOBAL ROTATION EQUIVARIANCE.

| Model | Para. (M) | MACs (G/s) | PESQ | SI-SDR (dB) | WOPD (↓) | PD (↓) |
|-------------------|-------------|------------|-------------|--------------|--------------|-------------|
| Griffin-Lim | - | - | 4.23 | -17.07 | 0.342 | 90.07 |
| DiffPhase | 65.6 | 3330 | 4.41 | -11.75 | 0.230 | 85.66 |
| MP-SENet Up.* | 1.99 | 38.80 | 4.60 | 14.64 | 0.058 | 11.38 |
| SEMamba* | 1.88 | 38.01 | 4.59 | 13.63 | 0.059 | 12.46 |
| Proposed (Small) | 0.90 | 22.89 | 4.61 | 16.03 | 0.044 | 8.47 |
| – break MPICM GRE | 0.90 | 22.89 | 4.61 | 14.99 | 0.048 | 9.64 |
| – break Attn. GRE | 0.90 | 22.89 | 4.61 | 15.67 | 0.048 | 9.16 |
| – break FFN. GRE | 0.90 | 22.89 | 4.60 | 14.97 | 0.050 | 9.67 |

To substantiate the hypothesis that GRE has contribution to the improved phase prediction, we designed specific model variants to examine the impact of deliberately breaking this constraint through two distinct modifications: (1) substituting the modulus in MPICM with the sum of real and imaginary part of the phase feature during interactive gating, thereby breaking the GRE property in the encoder and decoder; (2) inverting the sign of the phase query component (9) (i.e., $\text{Re}(\mathbf{Q}_{\text{pha}}) \rightarrow -\text{Re}(\mathbf{Q}_{\text{pha}})$), which fundamentally disrupts the GRE in the hybrid attention mechanism; and (3) remove

TABLE III
DENOISING PERFORMANCE EVALUATION ON THE
VOICEBANK+DEMAND TEST SET AND THE ZERO-SHOT DNS-2020
NON-REVERBERANT TEST SET. ALL MODELS WERE TRAINED
EXCLUSIVELY ON THE VBD CORPUS.

| Method | Para. (M) | PESQ | STOI | UT-MOS | DNS-MOS | PD (↓) | WOPD (↓) |
|------------------------------------|-------------|--------------|--------------|--------------|--------------|--------------|--------------|
| Test Set: VoiceBank+DEMAND | | | | | | | |
| FRCRN | 6.90 | 3.199 | 0.953 | 4.009 | 3.582 | 14.703 | 0.192 |
| CMGAN | 1.83 | 3.410 | 0.956 | 4.051 | 3.556 | 7.309 | 0.167 |
| DB-AIAT | 2.81 | 3.264 | 0.956 | 4.038 | 3.563 | 7.521 | 0.174 |
| MP-SENet | 2.05 | 3.496 | 0.960 | 4.045 | 3.557 | 7.315 | 0.162 |
| MP-SENet Up. | 2.26 | 3.604 | 0.961 | 4.064 | 3.563 | 7.403 | 0.163 |
| SEMamba | 2.25 | 3.564 | <u>0.960</u> | 4.041 | 3.549 | 7.443 | 0.164 |
| Proposed | 1.55 | 3.584 | 0.958 | 4.070 | 3.567 | 7.345 | 0.163 |
| Test Set: DNS-2020 Non-Reverberant | | | | | | | |
| CMGAN | 1.83 | 2.759 | 0.957 | 3.675 | 3.941 | 8.490 | 0.190 |
| MP-SENet | 2.05 | 2.719 | <u>0.960</u> | <u>3.697</u> | 3.930 | 8.423 | 0.185 |
| MP-SENet Up. | 2.26 | 2.790 | 0.959 | 3.591 | 3.897 | 8.271 | 0.181 |
| SEMamba | 2.25 | 2.440 | 0.938 | 3.438 | 3.862 | 9.455 | 0.204 |
| Proposed | 1.55 | 2.901 | 0.967 | 3.848 | 4.010 | 7.743 | 0.171 |

the modulus in (13) and apply GLU to real and imaginary components separately, which disrupts the GRE in phase FFN. As in Table II, all modifications resulted in evident degradation in phase accuracy, confirming that strict adherence to rotation equivariance is instrumental for precise phase modeling.

B. Speech Denoising on Benchmark Datasets

For denoising task, the model has to extract the distribution of clean speech from an unbounded, open set of noise distributions. Unlike the phase retrieval task, denoising presents a scenario where both magnitude and phase inputs are unreliable, particularly in low-SNR regions. Table III presents the results for models trained on the VoiceBank+DEMAND dataset. We benchmark against a diverse set of competitive baselines: the complex-valued FRCRN [56], the dual-branch methods DB-AIAT [33] and CMGAN [15], and the Mamba-based SEMamba [55]. Additionally, we compare against our direct architectural predecessors, MP-SENet [16] and MP-SENet Up. [18], to isolate the specific performance gains attributed to the dual-stream design rotation-equivariant phase modeling. Our method achieves competitive performance, securing top-tier results on non-intrusive metrics (DNSMOS and UTMOS), while maintaining only a marginal gap in intrusive metrics compared to MP-SENet Up. We attribute this discrepancy to the inherent limitations of the VBD corpus; It is very small-scaled, and recording environment acoustical factors presented in the “clean” reference targets can cause intrusive metrics to over-penalize valid enhancements. To rigorously validate generalization capability beyond this limited test set, we performed a cross-corpus evaluation by applying the VBD-trained model directly to the DNS non-reverberant test set. In this zero-shot setting, our method demonstrates significant superiority, surpassing all baselines on all metrics with gains exceeding 0.1 in PESQ, alongside an evident reduction in phase-related metrics. This proves that the proposed method is actually equipped with stronger denoising ability in un-

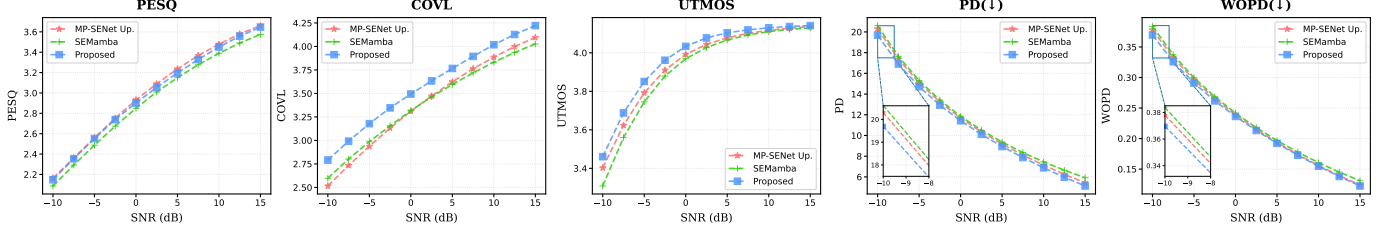


Fig. 4. Performance Comparison across varying SNRs. Models were trained on the DNS-2020 corpus and evaluated on re-mixed versions of the VoiceBank+DEMAND test set ranging from -10 dB to 15 dB.

seen acoustical scenarios, which underscores the value of our manifold-aware design, showing that the network is compelled to learn physically consistent magnitude and phase structures rather than memorizing spurious, dataset-specific patterns, thereby showing stronger robustness in unseen acoustic environments. Table IV presents the evaluation results on the

TABLE IV

COMPARATIVE EVALUATION OF MODELS TRAINED ON THE LARGE-SCALE DNS-2020 DATASET AND TESTED ON THE OFFICIAL NON-REVERBERANT BLIND TEST SET.

| Method | Para. (M) | PESQ | STOI | SI-SDR | UT-MOS | PD (↓) |
|--------------|-----------|--------------|--------------|---------------|--------------|--------------|
| Noisy | – | 1.582 | 0.915 | 9.230 | 2.365 | 9.333 |
| FRCRN | 6.90 | 3.233 | 0.977 | 19.783 | 3.911 | 7.432 |
| MFNet | – | 3.431 | 0.980 | 20.310 | 4.051 | 7.122 |
| MP-SENet Up. | 2.26 | 3.624 | 0.982 | 21.033 | 4.053 | 6.713 |
| SEMamba | 2.85 | 3.593 | 0.981 | 20.732 | 4.024 | 6.914 |
| Proposed | 1.55 | 3.645 | 0.982 | 21.060 | 4.068 | 6.571 |

large-scale DNS 2020 dataset. Consistent with previous findings, our method surpasses all baselines in phase estimation precision (PD and WOPD) while simultaneously achieving state-of-the-art results in perceptual quality metrics, including PESQ and UTMOS. This validates that despite the vast scale of the training data, our model (1.55 M parameters) effectively extracts high-fidelity speech distributions, outperforming larger baselines such as MP-SENet Up. (>2.2 M parameters). This confirms that appropriate manifold handling with Global Rotation Equivariance (GRE) in phase modeling provides a more effective inductive bias for speech enhancement than simply increasing model capacity.

To further investigate the capability of our method under varying acoustic conditions, we also conducted a cross-corpus validation. Specifically, we evaluated the model trained on the DNS dataset using the VBD test set, which was re-mixed at lower SNRs ranging from -10 dB to 15 dB, with the top-ranked SEMamba and MP-SENet Up. for comparison. As illustrated in Fig. 4, our method demonstrates consistent superiority in low-SNR scenarios, particularly evident in the COVL and UTMOS metrics. The phase-sensitive metrics (PD and WOPD) reveal distinct advantages, despite being relatively close overall. The evident improvements in perceptual quality and the slight improvement in phase accuracy demonstrate the resilience of our proposed method in mismatched and low-SNR environments, highlighting the distinct advantage of our phase modeling over the baselines.

C. Universal Speech Enhancement

While pure denoising at high SNRs relies predominantly on magnitude recovery, USE tasks involving DR and BWE put more focus on accurate phase reconstruction. In this part, we include the recently proposed ZipEnhancer [20] as another strong baseline, which utilizes multi-resolution resampling to optimize efficiency and performance, as well as the generative diffusion-based UniverseSE++ [57]. Since sigmoid-based masking [18] is not fit for the BWE-contained tasks, all predictive baselines are re-trained using a mapping method that employs a ReLU activation to ensure non-negative magnitude output [20], with consistent training configurations in Section IV-B. The params and computational cost comparison is in Table VI, quantitative evaluation results are detailed in Table V, and spectrogram comparisons are presented in Fig. 5. As in Table VI, our method achieves the lowest parameter count, and its computational cost is significantly lower than that of our structural baseline, MP-SENet Up, remaining comparable to distinct architectures like SEMamba and ZipEnhancer. Despite this efficiency, the proposed method demonstrates evident performance gains over these approaches. Readers are encouraged to audit the audio samples and training logs hosted on our project website.¹

In single-task evaluations, our method demonstrates consistent superiority over strong baselines. For all tasks, our method outperforms the structural baseline MP-SENet Up across all metrics with an evident margin. Notably, UniverseSE++ lags behind the proposed method in signal fidelity metrics (e.g., PESQ and SI-SDR) and phase accuracy (PD). We attribute this to the inherent stochasticity of generative processes, which can introduce phase inconsistencies that degrade waveform alignment and consequently impair perceptual quality. For DN, our method achieves the best result in PESQ and phase accuracy, achieving parity with ZipEnhancer while generating clearer harmonic structures as evidenced in the first row of Fig. 5. In DR, it secures the best performance across all metrics with significantly higher phase accuracy. In BWE, our model gets the top-tier performance comparable to ZipEnhancer, and shows a stronger ability to generate high-frequency speech components according to the third row of Fig. 5. The advantages of our approach are even more pronounced in the composite distortion scenarios, where our method achieves the best results across almost all metrics other than the second best in UTMOS for the DN+DR task. While the absolute im-

¹<https://wangchengzhong.github.io/RENet-Supplementary-Materials/>

TABLE V
PERFORMANCE COMPARISON FOR COMPOSITE SE TASKS (TRAIN: DNS-2021, TEST: WSJ0+WHAMR!).

| Task | Method | WB-PESQ (↑) | STOI (↑) | SI-SDR (↑) | COVL (↑) | UTMOS (↑) | PD (↓) | WOPD (↓) |
|-----------|-----------------|----------------|--------------|---------------|--------------|--------------|---------------|--------------|
| DN | UniverSE++ | 2.007 | 0.935 | 10.795 | 2.531 | 3.708 | 23.508 | 0.417 |
| | MP-SENet Up. | 2.656 | 0.951 | 14.898 | 3.481 | 3.903 | 12.467 | 0.261 |
| | SEMamba | 2.658 | 0.950 | 14.311 | 3.427 | 4.026 | 12.559 | 0.256 |
| | ZipEnhancer | 2.717 | 0.958 | 15.251 | <u>3.507</u> | 3.896 | <u>11.862</u> | <u>0.250</u> |
| | Proposed | 2.750 | <u>0.957</u> | <u>15.234</u> | 3.545 | <u>3.945</u> | 11.857 | 0.245 |
| DR | UniverSE++ | 2.565 | 0.944 | 6.043 | 2.978 | 3.735 | 28.692 | 0.494 |
| | MP-SENet Up. | 3.486 | 0.978 | 11.691 | 4.306 | 4.252 | 12.056 | 0.253 |
| | SEMamba | <u>3.577</u> | <u>0.981</u> | 12.143 | <u>4.347</u> | <u>4.249</u> | 10.548 | <u>0.221</u> |
| | ZipEnhancer | 3.501 | <u>0.981</u> | <u>12.502</u> | 4.344 | 4.224 | <u>10.432</u> | 0.224 |
| | Proposed | 3.662 | 0.987 | 13.960 | 4.472 | 4.263 | 8.878 | 0.190 |
| BWE | UniverSE++ | 3.257 | 0.954 | 11.243 | 3.413 | 3.943 | 24.034 | 0.356 |
| | MP-SENet Up. | 3.322 | 0.967 | 11.245 | 3.602 | 4.057 | 21.183 | 0.288 |
| | SEMamba | 3.305 | 0.967 | 10.992 | 3.561 | 4.058 | 22.186 | 0.306 |
| | ZipEnhancer | <u>3.486</u> | 0.971 | 11.517 | 3.932 | <u>4.073</u> | 20.685 | <u>0.287</u> |
| | Proposed | 3.560 | <u>0.969</u> | <u>11.453</u> | <u>3.915</u> | 4.110 | <u>20.949</u> | 0.286 |
| DN+DR | UniverSE++ | 1.730 | 0.879 | 4.219 | 2.291 | 3.070 | 36.290 | 0.603 |
| | MP-SENet Up. | 2.330 | 0.925 | 8.589 | 3.165 | 3.578 | 20.399 | 0.391 |
| | SEMamba | 2.372 | 0.929 | 8.747 | 3.160 | 3.792 | 19.365 | 0.364 |
| | ZipEnhancer | <u>2.401</u> | <u>0.935</u> | <u>9.204</u> | <u>3.196</u> | 3.683 | <u>18.847</u> | <u>0.359</u> |
| | Proposed | 2.444 | 0.936 | 9.660 | 3.263 | <u>3.733</u> | 18.095 | 0.344 |
| DN+DR+BWE | UniverSE++ | 1.610 | 0.871 | 3.938 | 2.117 | 2.987 | 39.195 | 0.634 |
| | MP-SENet Up. | 2.103 | 0.916 | 6.792 | 2.546 | 3.376 | 30.106 | 0.490 |
| | SEMamba | 2.066 | 0.921 | 6.617 | 2.712 | <u>3.581</u> | 29.371 | 0.485 |
| | ZipEnhancer | <u>2.169</u> | <u>0.926</u> | <u>7.116</u> | <u>2.815</u> | 3.538 | <u>29.100</u> | <u>0.476</u> |
| | Proposed | 2.206 | 0.928 | 7.407 | 2.831 | 3.598 | 28.413 | 0.462 |

TABLE VI
COMPARISON OF PARAMETERS AND COMPUTATIONAL COST

| Metric | ZipEnhancer | UniverSE++ | MP-SENet Up. | SEMamba | Proposed |
|--------------|--------------|------------|--------------|---------|-------------|
| Params (M) | 2.04 | 42.80 | 2.26 | 2.85 | 1.55 |
| MACs (G/sec) | 31.42 | 42.81 | 43.14 | 32.73 | 34.97 |

provements in perceptual metrics may appear incremental, we conducted a paired t-test between the scores of the proposed method and ZipEnhancer, the second-strongest baseline, across the composite tasks. The results confirm that the performance gains are statistically significant ($p < 0.01$) for all metrics except STOI¹. This superiority might stem from the fact that our deep magnitude-phase manifold separation and GRE-based phase modeling has the potential to map the hidden features in a better way. Conventional predictive methods may struggle to map inputs to unconstrained high-dimensional manifolds that become brittle when different degradation overlaps with each other. In contrast, the proposed network bypasses unrelated manifold regions and focus capacity on valid speech reconstruction efforts, leading to better overall performance with comparable costs and fewer parameters.

D. Ablation Studies

To ensure a rigorous evaluation, we focus on the composite DN+DR+BWE task for ablation studies, which represents the most complex degradation scenario. Firstly, as in the phase retrieval task (Section V-A), we also perform an ablation to validate the rationale behind our global rotation equivariant design in composite degradation case. As presented in Table

VII, all modifications that breaks the GRE lead to marked performance degradation. This confirms that GRE modeling serves as an effective inductive bias for phase processing, allowing the network to align more precisely with the intrinsic phase topology than conventional approaches. Notably, disrupting equivariance within the hybrid attention block incurs the most severe penalty, underscoring its pivotal role in phase modeling.

TABLE VII
IMPACT OF VIOLATING GLOBAL ROTATION EQUIVARIANCE (GRE) IN INDIVIDUAL NETWORK COMPONENTS ON MODEL PERFORMANCE.

| Model | PESQ | STOI | UTMOS | PD(↓) | WOPD(↓) |
|-------------------|-------|-------|-------|--------|---------|
| Proposed | 2.206 | 0.928 | 3.598 | 28.413 | 0.462 |
| – break MPICM GRE | 2.049 | 0.917 | 3.395 | 29.711 | 0.493 |
| – break Attn. GRE | 2.026 | 0.915 | 3.265 | 31.395 | 0.510 |
| – break FFN GRE | 2.061 | 0.919 | 3.302 | 29.390 | 0.482 |

We further investigate the impact of different convolutional channel configurations (Table VIII). As expected, increasing channel depth generally improves performance; we selected the 48/16 configuration for its balance between efficiency and quality. Notably, even our largest configuration maintains a lower computational cost than MP-SENet Up. While reducing the capacity of either stream leads to degradation, shrinking the magnitude stream (e.g., 32/24) has a more pronounced impact than reducing the phase stream (48/16). This aligns with the primary role magnitude plays in speech perception. However, by isolating the circular phase topology, our architecture effectively removes phase-induced interference, enhancing magni-

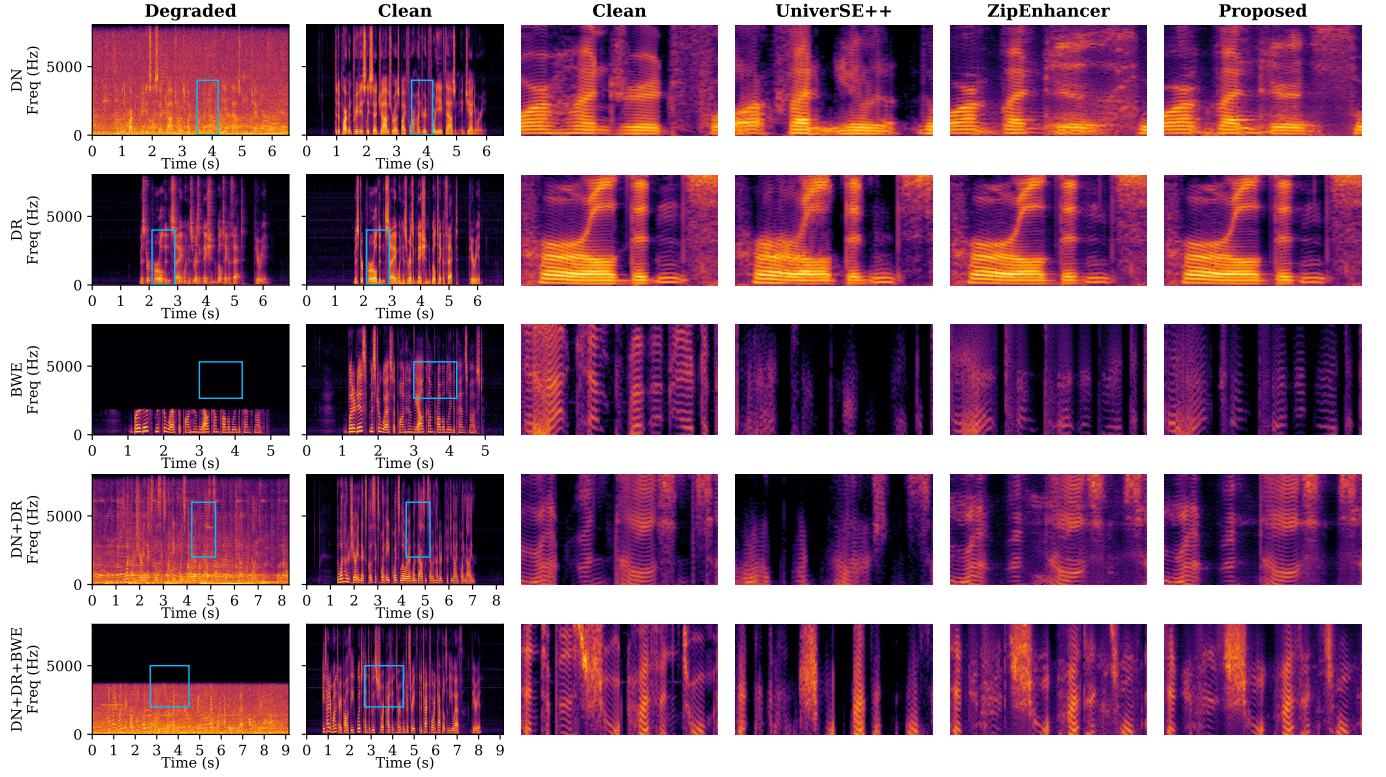


Fig. 5. Spectrogram visualization of enhanced speech under diverse distortion scenarios. The audio files are taken from WSJ0+WHAMR! test set.

tude modeling as evidenced by superior magnitude-dominated STOI scores reported before.

TABLE VIII

AN INVESTIGATION OF DIFFERENT CHANNEL CONFIGURATIONS.

| Channels Conf. ($C_{\text{mag}} / C_{\text{pha}}$) | Para. (M) | MACs (G/sec) | PESQ | STOI | PD(\downarrow) |
|--|-------------|--------------|--------------|--------------|--------------------|
| 48 / 16 (Proposed) | 1.55 | 34.97 | 2.206 | 0.928 | 28.413 |
| 32 / 16 | 0.90 | 22.89 | 2.038 | 0.917 | 30.183 |
| 32 / 24 | 1.14 | 31.39 | 2.091 | 0.925 | 29.117 |
| 48 / 24 | 1.78 | 42.72 | 2.174 | 0.930 | 27.790 |

Next, we investigate the specific internal design choices of the MPICM. First, we validate the efficacy of the interactive gating mechanism by removing the cross-stream interaction entirely. As indicated in Table IX, this ablation results in a noticeable performance drop, confirming that the explicit exchange of information enables the two streams to mutually refine their latent magnitude and phase representations. We also analyze the impact of the normalization strategy. While Complex RMS Norm is adopted for the phase branch to maintain GRE, we tested replacing the RMS Normalization in the magnitude branch with standard Instance Normalization. This change resulted in a performance decline. The rationale of this phenomenon may lie in the non-negative magnitude input. Instance Normalization subtracts the mean, making the distribution center at zero in the very first layer, and may cause information loss when activated by SiLU. In contrast, RMS Normalization re-scales the energy and only alters the sign

via bias, making it more stable for preserving the integrity of magnitude information in our separated magnitude-phase stream setting.

TABLE IX
COMPONENT-WISE ABLATION STUDY OF THE MPICM AND HADF.

| Model | PESQ | STOI | UTMOS | PD(\downarrow) | WOPD(\downarrow) |
|--------------------------|-------|-------|-------|--------------------|----------------------|
| Proposed | 2.206 | 0.928 | 3.598 | 28.413 | 0.462 |
| -w/o gating | 2.097 | 0.918 | 3.495 | 29.817 | 0.490 |
| - MS* InstanceNorm | 2.069 | 0.920 | 3.330 | 29.149 | 0.481 |
| - w/o PS* Freq-wise Norm | 2.105 | 0.925 | 3.531 | 28.725 | 0.470 |
| - Naive Transformer-GRU | 1.995 | 0.909 | 3.126 | 31.236 | 0.512 |
| - Merge Attention | 2.093 | 0.924 | 3.445 | 29.153 | 0.472 |
| - GRU-based Comp. FFN | 2.049 | 0.918 | 3.295 | 29.646 | 0.485 |

* MS/PS: Magnitude/Phase Stream.

Turning to the bottleneck architecture, we first evaluate the necessity of our specialized dual-stream design by replacing the entire HADF module with the original, unified bottleneck from MP-SENet Up. As shown in Table IX, this reversion causes a significant performance degradation. This confirms that simply relying on general block to model the magnitude-phase dependencies is insufficient for manifold-aware encoder-decoder. Next, we investigated the attention mechanism by evaluating a ‘Merged Attention’ strategy. In this configuration, complex-valued phase features are mapped to the real domain via the modulus operation, concatenated with the magnitude features, and processed through a shared standard attention layer before branching into separate FFNs where the phase FFN uses the learned attention map to gate the complex

features. The evident decline in all metrics indicates that collapsing the complex phase representation into a generic real-valued feature vector results in information loss, and the phase stream benefits from strictly preserving its complex-valued nature. This validates our Hybrid Attention design, which effectively unifies the confidence of both streams without compromising the geometric integrity. Finally, we evaluate the design of phase FFN by replacing the convolution pipeline with a GRU-based structure, analogous to that used in the magnitude branch. To mitigate the implementation complexity of a fully complex-valued GRU, we employed a real-valued GRU approximation operating on concatenated real and imaginary components. Empirical results demonstrate that our proposed convolutional phase FFN outperforms this recurrent alternative. This suggests that the phase stream benefits from the locality inherent in convolution operations.

E. Visualization of the Attention Map

Finally, we visualize the attention maps from the HADF to analyze the internal mechanism of information fusion. We selected a representative frame containing a sustained voiced segment to highlight clear harmonic structures and plot its 2nd frequency-HADF attention map. By explicitly extracting the learned patterns from the magnitude and phase projections, distinct characteristics emerge, as shown in Fig. 6: the magnitude attention exhibits a structured distribution, capturing harmonic correlations and energy-based spectral dependencies across frequency bins. In contrast, the phase attention reveals a distinct periodic pattern, reflecting the angular similarities inherent to the circular manifold. For comparison, we analyzed the attention state of the same frame in MP-SENet Up., identifying the attention head with the closest pattern alignment to our learned features. Remarkably, its attention map shares a high degree of structural similarity with our magnitude pattern, indicating that joint mag-phase attention primarily captures energy-driven dependencies. However, the deviation of our composite Hybrid Attention score from the baseline map suggests that our method actively injects phase symmetry into the energy attention structure, which effectively allows the network to synthesize a dual-perspective representation.

VI. CONCLUSION

In this paper, we have proposed a manifold-aware framework for speech enhancement that fundamentally rethinks phase modeling through the lens of its intrinsic circular topology, introducing a Global Rotation Equivariant architectural design. By strictly enforcing geometric constraints on the phase stream and enabling information exchange via the MPICM and HADF modules, our approach effectively eliminates the coordinate-system dependency for phase modeling inherent in conventional networks. Extensive evaluations across phase retrieval, denoising, and universal speech restoration tasks demonstrate that our method achieves state-of-the-art performance with superior phase reconstruction accuracy and generalization capability, all while maintaining comparable computational efficiency. Thorough ablations confirm that global rotation equivariance is an effective inductive bias to

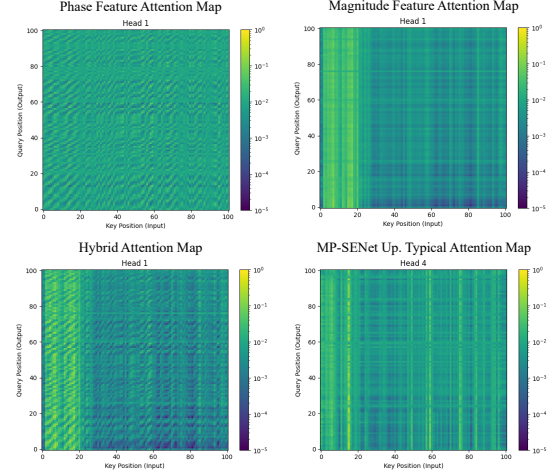


Fig. 6. Visualization of learned attention patterns for a voiced speech segment. (Upper Left) The attention component derived solely from the phase stream. (Upper Right) The attention component derived from the magnitude stream. (Lower Left) The proposed Hybrid Attention map (fused). (Lower Right) The most correlated attention head from the MP-SENet Up. baseline.

learn the intrinsic circular manifold of phase. Future work will investigate the extension of this rotation-equivariant paradigm to causal architectures for real-time processing applications.

REFERENCES

- [1] Y. Ephraim and D. Malah, "Speech enhancement using a minimum-mean square error short-time spectral amplitude estimator," *IEEE Trans. Acoust., Speech, Signal Process.*, vol. 32, no. 6, pp. 1109–1121, 1984.
- [2] I. Cohen and B. Berdugo, "Speech enhancement for non-stationary noise environments," *Signal Process.*, vol. 81, no. 11, pp. 2403–2418, 2001.
- [3] Y. Wang, A. Narayanan, and D. Wang, "On training targets for supervised speech separation," *IEEE/ACM Trans. Audio, Speech, Lang. Process.*, vol. 22, no. 12, pp. 1849–1858, 2014.
- [4] Y. Xu, J. Du, L.-R. Dai, and C.-H. Lee, "A regression approach to speech enhancement based on deep neural networks," *IEEE/ACM Trans. Audio, Speech, Lang. Process.*, vol. 23, no. 1, pp. 7–19, 2014.
- [5] C. Zheng, H. Zhang, W. Liu, X. Luo, A. Li, X. Li, and B. C. J. Moore, "Sixty years of frequency-domain monaural speech enhancement: From traditional to deep learning methods," *Trends Hear.*, vol. 27, p. 23312165231209913, 2023.
- [6] A. Li, W. Liu, C. Zheng, C. Fan, and X. Li, "Two heads are better than one: A two-stage complex spectral mapping approach for monaural speech enhancement," *IEEE/ACM Trans. Audio, Speech, Lang. Process.*, vol. 29, pp. 1829–1843, 2021.
- [7] M. Maciejewski, G. Wichern, E. McQuinn, and J. Le Roux, "WHAMR!: Noisy and reverberant single-channel speech separation," in *Proc. IEEE Int. Conf. Acoust., Speech Signal Process.*, 2020, pp. 696–700.
- [8] D. Wang and J. Lim, "The unimportance of phase in speech enhancement," *IEEE Trans. Acoust., Speech, Signal Process.*, vol. 30, no. 4, pp. 679–681, 1982.
- [9] K. Paliwal, K. Wójcicki, and B. Shannon, "The importance of phase in speech enhancement," *Speech Commun.*, vol. 53, no. 4, pp. 465–494, 2011.
- [10] A. Li, C. Zheng, R. Peng, and X. Li, "On the importance of power compression and phase estimation in monaural speech dereverberation," *JASA Express Lett.*, vol. 1, no. 1, p. 014802, Jan. 2021. [Online]. Available: <https://doi.org/10.1121/10.0003321>
- [11] Y.-X. Lu, Y. Ai, H.-P. Du, and Z.-H. Ling, "Towards high-quality and efficient speech bandwidth extension with parallel amplitude and phase prediction," *IEEE/ACM Trans. Audio, Speech, Lang. Process.*, vol. 33, pp. 236–250, 2025.
- [12] T. Gerkmann, M. Krawczyk-Becker, and J. Le Roux, "Phase processing for single-channel speech enhancement: History and recent advances," *IEEE Signal Process. Mag.*, vol. 32, no. 2, pp. 55–66, 2015.

[13] D. Yin, C. Luo, Z. Xiong, and W. Zeng, "PHASEN: A phase-and-harmonics-aware speech enhancement network," in *Proc. AAAI Conf. Artif. Intell.*, vol. 34, no. 05, 2020, pp. 9458–9465.

[14] G. Yu, A. Li, C. Zheng, Y. Guo, Y. Wang, and H. Wang, "Dual-branch attention-in-attention transformer for single-channel speech enhancement," in *Proc. IEEE Int. Conf. Acoust., Speech Signal Process.*, 2022, pp. 761–765.

[15] S. Abdulatif, R. Cao, and B. Yang, "CMGAN: Conformer-based metric-GAN for monaural speech enhancement," *IEEE/ACM Trans. Audio, Speech, Lang. Process.*, vol. 32, pp. 2477–2493, 2024.

[16] Y.-X. Lu, Y. Ai, and Z.-H. Ling, "MP-SENet: A speech enhancement model with parallel denoising of magnitude and phase spectra," in *Proc. Interspeech*, 2023, pp. 3834–3838.

[17] Y. Ai and Z.-H. Ling, "Neural speech phase prediction based on parallel estimation architecture and anti-wrapping losses," in *Proc. IEEE Int. Conf. Acoust., Speech Signal Process.*, 2023, pp. 1–5.

[18] Y.-X. Lu, Y. Ai, and Z.-H. Ling, "Explicit estimation of magnitude and phase spectra in parallel for high-quality speech enhancement," *Neural Netw.*, vol. 189, p. 107562, 2025.

[19] J. Wang, Z. Lin, T. Wang, M. Ge, L. Wang, and J. Dang, "Mamba-SEUNet: Mamba UNet for monaural speech enhancement," in *Proc. IEEE Int. Conf. Acoust., Speech Signal Process.*, 2025, pp. 1–5.

[20] H. Wang and B. Tian, "ZipEnhancer: Dual-path down-up sampling-based zipformer for monaural speech enhancement," in *Proc. IEEE Int. Conf. Acoust., Speech Signal Process.*, 2025, pp. 1–5.

[21] Y. Hu, Q. Yang, W. Wei, L. Lin, L. He, Z. Ou, and W. Yang, "MNN-Net: Speech enhancement network via modeling the noise," *IEEE/ACM Trans. Audio, Speech, Lang. Process.*, vol. 33, pp. 1208–1219, 2025.

[22] X. Xu, W. Tu, Y. Yang, J. Li, and Y. Zhang, "Interactive target positive and negative features modeling for monaural speech enhancement," *IEEE/ACM Trans. Audio, Speech, Lang. Process.*, vol. 33, pp. 4856–4869, 2025.

[23] Y. Hu, Y. Liu, S. Lv, M. Xing, S. Zhang, Y. Fu, J. Wu, B. Zhang, and L. Xie, "DCCRN: Deep complex convolution recurrent network for phase-aware speech enhancement," in *Proc. Interspeech*, 2020, pp. 2472–2476.

[24] N. B. Thien, Y. Wakabayashi, K. Iwai, and T. Nishiura, "Inter-frequency phase difference for phase reconstruction using deep neural networks and maximum likelihood," *IEEE/ACM Trans. Audio, Speech, Lang. Process.*, vol. 31, pp. 1667–1680, 2023.

[25] S. Zhang, Z. Qiu, D. Takeuchi, N. Harada, and S. Makino, "Unrestricted global phase bias-aware single-channel speech enhancement with conformer-based metric GAN," in *Proc. IEEE Int. Conf. Acoust., Speech Signal Process.*, 2024, pp. 1026–1030.

[26] Y. Masuyama, K. Yatabe, Y. Koizumi, Y. Oikawa, and N. Harada, "Phase reconstruction based on recurrent phase unwrapping with deep neural networks," in *Proc. IEEE Int. Conf. Acoust., Speech, Signal Process.*, Barcelona, Spain, 2020, pp. 726–730.

[27] D. C. Ghiglia and M. D. Pritt, *Two-Dimensional Phase Unwrapping: Theory, Algorithms, and Software*. New York, NY, USA: Wiley, 1998.

[28] F. Liu, Y. Ai, Y.-X. Lu, R.-C. Zheng, H.-P. Du, and Z.-H. Ling, "Universal discrete-domain speech enhancement," *IEEE Trans. Audio Speech Lang. Process.*, vol. 34, pp. 285–298, 2026.

[29] E. Huang, Z. Zhang, T. Xu, C. Xia, K. Hu, Y. Yang, T. Pan, D. Dong, and Z. Qin, "Holographic transformers for complex-valued signal processing: Integrating phase interference into self-attention," *arXiv*, 2025.

[30] S. Maitra and B. Yegnanarayana, "Spectral-envelope and group-delay models for transient signals—applications to castanets and stop consonants," in *Proc. IEEE Int. Conf. Acoust., Speech, Signal Process.*, 2011, pp. 4412–4415.

[31] H. A. Murthy and B. Yegnanarayana, "Group delay functions and its applications in speech technology," *Sādhanā*, vol. 36, no. 5, pp. 745–782, 2011.

[32] C. Lee, H. Hasegawa, and S. Gao, "Complex-valued neural networks: A comprehensive survey," *IEEE/CAA J. Autom. Sinica*, vol. 9, no. 8, pp. 1406–1426, 2022.

[33] G. Yu, A. Li, H. Wang, Y. Wang, Y. Ke, and C. Zheng, "DBT-Net: Dual-branch federative magnitude and phase estimation with attention-in-attention transformer for monaural speech enhancement," *IEEE/ACM Trans. Audio, Speech, Lang. Process.*, vol. 30, pp. 2629–2644, 2022.

[34] B. Zhang and R. Sennrich, "Root mean square layer normalization," *Proc. Adv. Neural Inf. Process. Syst. (NeurIPS)*, vol. 32, 2019.

[35] F. Eilers and X. Jiang, "Building blocks for a complex-valued transformer architecture," in *Proc. IEEE Int. Conf. Acoust., Speech Signal Process.*, 2023, pp. 1–5.

[36] K. Wang, B. He, and W.-P. Zhu, "TSTNN: Two-stage transformer based neural network for speech enhancement in the time domain," in *Proc. IEEE Int. Conf. Acoust., Speech Signal Process.*, 2021, pp. 7098–7102.

[37] C. V. Botinhao, X. Wang, S. Takaki, and J. Yamagishi, "Investigating RNN-based speech enhancement methods for noise-robust text-to-speech," in *Proc. ISCA Speech Synth. Workshop*, 2016, pp. 159–165.

[38] C. K. Reddy, V. Gopal, R. Cutler, E. Beyrami, R. Cheng, H. Dubey, S. Matusevych, R. Aichner, A. Aazami, S. Braun, P. Rana, S. Srinivasan, and J. Gehrke, "The INTERSPEECH 2020 deep noise suppression challenge: Datasets, subjective testing framework, and challenge results," in *Proc. Interspeech*, 2020, pp. 2492–2496.

[39] C. Veaux, J. Yamagishi, and S. King, "The voice bank corpus: Design, collection and data analysis of a large regional accent speech database," in *Proc. Orient. Cocosda*, 2013, pp. 1–4.

[40] J. Thiemann, N. Ito, and E. Vincent, "The diverse environments multi-channel acoustic noise database (DEMAND): A database of multichannel environmental noise recordings," in *Proc. Meet. Acoust.*, vol. 19, no. 1, 2013, p. 035081.

[41] C. K. A. Reddy, H. Dubey, V. Gopal, R. Cutler, S. Braun, H. Gamper, R. Aichner, and S. Srinivasan, "ICASSP 2021 deep noise suppression challenge," in *Proc. IEEE Int. Conf. Acoust., Speech Signal Process.*, 2021, pp. 6623–6627.

[42] J. S. Garofolo *et al.*, "CSR-I (WSJ0) Complete," LDC93S6A, 1993. [Online]. Available: <https://catalog.ldc.upenn.edu/LDC93S6A>

[43] J. B. Allen and D. A. Berkley, "Image method for efficiently simulating small-room acoustics," *J. Acoust. Soc. Amer.*, vol. 65, no. 4, pp. 943–950, 1979.

[44] J. Kong, J. Kim, and J. Bae, "HiFi-GAN: Generative adversarial networks for efficient and high fidelity speech synthesis," *Proc. Adv. Neural Inf. Process. Syst. (NeurIPS)*, vol. 33, pp. 17 022–17 033, 2020.

[45] L. Dai, A. Li, Z. Han, C. Zheng, and X. Li, "BAPEN: Towards versatile audio phase retrieval," in *Proc. ACM Int. Conf. Multimedia*, 2025, pp. 8293–8302.

[46] H.-S. Choi, J.-H. Kim, J. Huh, A. Kim, J.-W. Ha, and K. Lee, "Phase-aware speech enhancement with deep complex U-Net," in *Proc. Int. Conf. Learn. Represent. (ICLR)*, 2019.

[47] A. W. Rix, J. G. Beerends, M. P. Hollier, and A. P. Hekstra, "Perceptual evaluation of speech quality (PESQ) – a new method for speech quality assessment of telephone networks and codecs," in *Proc. IEEE Int. Conf. Acoust., Speech Signal Process.*, vol. 2, 2001, pp. 749–752.

[48] C. H. Taal, R. C. Hendriks, R. Heusdens, and J. Jensen, "A short-time objective intelligibility measure for time-frequency weighted noisy speech," in *Proc. IEEE Int. Conf. Acoust., Speech Signal Process.*, 2010, pp. 4214–4217.

[49] Y. Hu and P. C. Loizou, "Evaluation of objective quality measures for speech enhancement," *IEEE Trans. Audio Speech Lang. Process.*, vol. 16, no. 1, pp. 229–238, 2008.

[50] J. Le Roux, S. Wisdom, H. Erdogan, and J. R. Hershey, "SDR – half-baked or well done?" in *Proc. IEEE Int. Conf. Acoust., Speech Signal Process.*, 2019, pp. 626–630.

[51] C. K. Reddy, V. Gopal, and R. Cutler, "DNSMOS: A non-intrusive perceptual objective speech quality metric to evaluate noise suppressors," in *Proc. IEEE Int. Conf. Acoust., Speech Signal Process.*, 2021, pp. 6493–6497.

[52] T. Saeki, D. Xin, W. Nakata, T. Koriyama, S. Takamichi, and H. Saruwatari, "UTMOS: UTokyo-SaruLab system for VoiceMOS challenge 2022," in *Proc. Interspeech*, 2022, pp. 4521–4525.

[53] D. Griffin and J. Lim, "Signal estimation from modified short-time Fourier transform," *IEEE Trans. Acoust., Speech, Signal Process.*, vol. 32, no. 2, pp. 236–243, 1984.

[54] T. Peer, S. Welker, and T. Gerkmann, "DiffPhase: Generative diffusion-based STFT phase retrieval," in *Proc. IEEE Int. Conf. Acoust., Speech Signal Process.*, 2023, pp. 1–5.

[55] R. Chao, W.-H. Cheng, M. La Quatra, S. M. Siniscalchi, C.-H. H. Yang, S.-W. Fu, and Y. Tsao, "An investigation of incorporating mamba for speech enhancement," in *Proc. IEEE Spoken Lang. Technol. Workshop (SLT)*, 2024, pp. 302–308.

[56] S. Zhao, B. Ma, K. N. Watcharasupat, and W.-S. Gan, "FRCRN: Boosting feature representation using frequency recurrence for monaural speech enhancement," in *Proc. IEEE Int. Conf. Acoust., Speech Signal Process.*, 2022, pp. 9281–9285.

[57] R. Scheibler, Y. Fujita, Y. Shirahata, and T. Komatsu, "Universal score-based speech enhancement with high content preservation," in *Proc. Interspeech*, 2024, pp. 1165–1169.